A CO2 sink in a tropical coastal lagoon impacted by cultural eutrophication and upwelling

Thaís Erbas, Aguinaldo Marques, Gwenaël Abril

A CO_2 sink in a tropical coastal lagoon impacted by cultural eutrophication and upwelling

Thaís Erbas[1], Aguinaldo Marques[1] and Gwenaël Abril[1,2]

[1]Universidade Federal Fluminense (UFF), Instituto de Biologia, Programa de Pós-Graduação em Biologia Marinha e Ambientes Costeiros (PBMAC), Niterói, RJ, 24020-971, Brazil

[2]Laboratoire de Biologie des Organismes et Ecosystèmes Aquatiques (BOREA), Muséum National d'Histoire Naturelle, UMR 8067, CNRS, MNHN, IRD, SU, UCN, UA, Paris, France.

Submitted to Estuarine Coastal and Shelf Science, revised version.

Abstract

Tropical coastal lagoons are recognized as very productive ecosystems. However, very little is known on the direction and magnitude of their CO_2 exchange with the atmosphere. We report on air-water CO_2 fluxes and carbon concentrations in a tropical shallow lagoon impacted by cultural eutrophication. During two contrasting field surveys, the first in Nov. 2019 during dry conditions and the second in Feb. 2020 during wet summer condition and intrusion of coastal upwelling waters inside the lagoon. At both seasons, spatial *in situ* monitoring of temperature, salinity and partial pressure of CO_2 (pCO_2) reveal the presence of undersaturated pCO_2 values (between 60 and 300 ppmv), uptake of atmospheric CO_2 (between 0.9 and 9.2 mmol m^{-2} h^{-1}) inside the lagoon, at salinities between 10 and 32. Temporal monitoring data at the mouth of the lagoon throughout tidal cycles revealed the entrance of cold South Atlantic Central Waters (SACW) from the Cabo Frio's upwelling during flood tides in Feb. 2020 but not in Nov. 2019. The cold SACW with temperatures down to 16°C were supersaturated in CO_2 (pCO_2 about 520 ppmv) and a CO_2 source to the atmosphere (between 0.2 and 1.4 mmol m^{-2} h^{-1}). During mixing of this SACW in the most marine compartment of the lagoon, the biological CO_2 uptake and enhanced autotrophy overcame the effect of degassing SACW waters by heating. For both cruises, a consistent landward trend consisted in a decrease in pCO_2 and dissolved inorganic carbon (DIC) mirrored by an increase of dissolved organic carbon (DOC) (between 4.6 and 19.8 mg L^{-1}), particulate organic carbon (POC) (between 3.3 and 12.3 mg L^{-1}), and chlorophyll a (Chl *a*) (between 7.6 and 217 µg L^{-1}). POC, DOC and Chl *a* and the POC:Chl *a* ratio suggest that, organic carbon in the lagoon is a mixture of phytoplankton biomass produced in the lagoon, domestic wastewater loaded from multiple point sources and pulsated inputs from small rivers. Our study in the Saquarema lagoon confirms recent works in other densely populated tropical coastal ecosystems, revealing that eutrophication enhances the autotrophy of shallow tropical lagoons, making them act as efficient factories for atmospheric CO_2 absorption and organic carbon storage in sediments and export to the ocean.

Keywords

partial pressure of CO_2, autotrophy, carbon dynamics, tropical shallow lagoon

1 Introduction

The growing concern about the impact of anthropogenic carbon dioxide (CO_2) emissions has intensified research of organic and inorganic carbon fluxes through and within ecosystems. The coastal environments, require particularly precise quantification as they are highly dynamic components of the global carbon cycle and budget (Cai 2011; Borges and Abril 2011; Bauer et al. 2013). Although the global estuarine area is modest, these ecosystems have the capacity to emit a quantity of CO_2 that substantially offsets the of CO_2 sink on the continental shelves (Borges 2005; Borges et al. 2005; Cai et al. 2006; Chen and Borges 2009). However, owing to their strong intrinsic heterogeneity, coastal ecosystems are still poorly documented in terms of CO_2 exchange, especially in the tropics. Despite their modest surface area, compared to the ocean, coastal environments such as estuaries, mangroves, lagoons and bays, play a fundamental role in marine primary production, remineralization and sedimentation of organic carbon, and global air-sea CO_2 exchange (Wollast 1991; Sabine et al. 2004; Borges 2005; Cai 2011). In most estuaries, *i.e.* in semi-enclosed water bodies where freshwater mixes with seawater (Pritchard 1967), total ecosystem respiration generally exceeds gross primary production. As a result, estuaries are generally net heterotrophic and sources of atmospheric CO_2 (Gattuso et al. 1998; Borges and Abril 2011). This conclusion was reached on the basis of intensive works in estuaries with geographically well-defined salinity gradients. These "funnel-type estuaries" receive significant inputs of terrestrial organic matter from the rivers that fuel heterotrophic respiration, while primary production is limited by the availability of light due to the high turbidity, and despite a large availability of nutrients (Borges and Abril 2011). In general, low salinity regions are highly heterotrophic, oxygen depleted and strong CO_2 sources (Frankignoulle et al. 1998), whereas at high salinity, estuarine and marine phytoplankton can grow, reduce CO_2 degassing flux and, in some cases, generate uptake of atmospheric CO_2 (Körtzinger 2003; Jiang et al. 2008; Borges and Abril 2011). Some recent works in tropical regions have reported different patterns of CO_2 fluxes, with strong sinks of atmospheric CO_2 induced by eutrophication and/or by thermodynamic mixing of poorly buffered freshwaters with seawater (Cotovicz et al. 2015; 2020; 2021; Abril et al. 2021). Estuaries, lagoons and tropical bays have their specific characteristics, and will also present specific properties with respect of carbon cycling and CO_2 fluxes, very different from those from temperate and boreal estuaries.

Tropical coastal lagoons are particularly under-sampled for CO_2 fluxes (Chen et al. 2013), and only a couple of studies document the carbon cycle, carbonate chemistry and CO_2 fluxes, in these types of estuaries (Koné et al. 2008; Ávila-López et al. 2016). Tropical coastal lagoons are characterized by

shallow depths, important intrusion of ocean water with tides, variable inputs of freshwater, and high productivity, both planktonic and benthic (Knoppers and Kjerfve 1999). In the most developing countries, the eutrophication is generated by anthropogenic nutrient inputs from untreated wastewater from sewage and industry (Nixon 1995). An example is lagoons in the tropics that suffer from anthropogenic pressure, and particularly from cultural eutrophication induced by sewage loads (Knoppers et al. 1999; Cerda et al. 2013). Eutrophication can create conditions for strong CO_2 uptake, as in densely populated tropical coastal embayments (Cotovicz et al. 2015; Kubo et al. 2017). In addition to biological activity, drastic changes in temperature occur in tropical lagoons, induced by the intrusion of cold marine waters and strong surface heating (Chen et al. 2013; Cotovicz et al. 2020). These thermal variations have the potential to generate important changes in the distributions of water partial pressure of CO_2 (pCO_2) and CO_2 fluxes at the air-sea interface (Ávila-López et al. 2016; Ribas Ribas et al. 2011; Cotovicz et al. 2020). The aim of this paper is to present original data of air-water CO_2 fluxes and inorganic and organic carbon distribution in a small shallow lagoon in the region of Rio de Janeiro in Brazil, impacted by eutrophication and seasonally influenced by cold marine waters coming from the upwelling of Cabo Frio (Castelão and Barth 2006). Our study includes high spatial and temporal resolution data of pCO_2 and the carbonate system, as well as organic carbon and chlorophyll concentrations, during two very contrasting periods with and without the intrusion of upwelling cold waters in the lagoon. The objectives are, first, to describe spatially and quantitatively the CO_2 exchanges between the lagoon and the atmosphere; second, to relate the air-lagoon CO_2 fluxes to the variations of other inorganic and organic carbon species, as well as the lateral exchanges with the ocean; third, to discuss on the light our work as well as other recent studies, how eutrophication is becoming a predominant driver of the carbon cycle and air-sea CO_2 exchange in densely populated tropical coastlines.

2 Materials and Methods

2.1 Study Area

The Saquarema Lagoon system is located on the southeast coast of Brazil, in the city of Saquarema at 73km of Rio de Janeiro city (Fig. 1), with a population estimated of 89 thousands of inhabitants (IBGE 2020). The lagoon has a total surface area of 21.2 km², with four different compartments called Mombaça (12.6 km²), Jardim (2 km²), Boqueirão (0.6 km²) and Fora (6 km²) and is permanently connected to the sea by a sand bar (Knoppers and Kjerfve 1999). This channel has been artificially opened to minimize impacts of pollution (located in Fora sub-lagoon). The mean depth of the lagoon is 1.2m and the drainage basin total area is 215 km² (Oliveira 2013). Many small rivers discharge

freshwater in the lagoon. Among these rivers, the Mato Grosso River that ends in the Urussanga Lagoon (Fig. 1) is the biggest, however the value of the total freshwater discharge by all the small rivers is unknown (Alves 2003). The tides in the region are microtidal and semidiurnal, averaging 0.5 m and 1.5 m in amplitude during neap tide and spring conditions, respectively (Alves 2003). In spring and summer, the Fora Lagoon receives cold and nutrient rich waters of the Cabo Frio coastal upwelling of South Atlantic Central Water (SACW, T< 18.0^{o}C and S 34.4 - 36.0). The region has a wet tropical climate, subject to orographic rains that occur most often from October to March. The prevailing winds are from the East and Northeast or winds from the south quadrant during cold fronts. The residence time of water in the system is 56 to 58 days in the Mombaça compartment, 48 to 56 days in the Jardim compartment, 20 to 48 days in the Boqueirão compartment and from 0 to 20 days in the Fora compartment, which has a connection to the sea (Alves 2003). The Saquarema lagoon system is undergoing a process of cultural eutrophication, which has been intensified by the accelerated urbanization that occurred since the 1970s and a lack of effective wastewater treatment (Knoppers et al. 1999).

2.2. Sampling Strategy

Two sampling campaigns were carried out during two contrasted climatic situations in Nov. 2019 and Feb. 2020. Both sampling corresponded to spring tide conditions (amplitudes respectively 1m and 1.1m). However, Nov. 2019 sampling occurred during the intrusion of a cold front coupled to an extratropical cyclone that enhance humidity in the region, causing strong S-SW winds and intensives rains during the preceding and sampling days. In opposite, Feb. 2020 sampling occurred during well established summer conditions, with high solar radiation and the persistence of strong northeast NE winds, generating intense upwelling of South Atlantic central waters (Castelão and Barth 2006; Coelho-Souza et al. 2012). During the two campaigns, the sampling strategies consisted in spatial surveys at daytime covering the major area of the lagoon using a small boat, with continuous measurements and discrete sampling (Fig. 2). Continuous measurements included the pCO_2, salinity, temperature, and position were measured *in situ* at a frequency of 1 min. Discrete sampling was performed along the continuous trails at 16 (in Nov. 2019) to 20 (in Feb. 2020) stations (Fig. 1). Another sampling strategy used was the temporal sampling at a fixed point in the channel at the mouth of the lagoon (Fig. 1) for 13 hours (one tidal cycle) in Nov. 2019 and for 25 hours (two tidal cycles) in February 2020. During this temporal sampling we used the aforementioned continuous measurements and hourly discrete sampling. Surface water samples were collected at approximately 20 cm depth in clean polypropylene 2 L bottles and then kept cooled in the dark for filtration within

the following five hours. Three rivers including the major contributor Mato Grosso River (Fig. 1) were reached by car the same day as the temporal monitoring at the mouth.

2.3. Analytical procedures

2.3.1. Continuous Measurements

For continuous measurements, water was pumped from ~20cm below the water surface at a flow of about 5 L min^{-1}. About 2 L min^{-1} to an equilibrator system and the rest to a flow-through customized acrylic chamber containing an YSI 6600 multiparameter probe to measure temperature and salinity. The salinity probe was calibrated with IAPSO standard seawater and deionized water. The marble equilibrator (Frankignoulle et al. 2001; Abril et al. 2006; Cotovicz et al. 2016) consisted in an acrylic tube filled with glass marbles where water flows from the top, and a closed air circuit with a flux of about (1 L min^{-1}), flowing in the opposite direction from the bottom to the top. The air is dried with drierite and pumped to a non-dispersive infrared (NDIR) gas analyser (LICOR LI- 820). Before and after each sampling campaigns, the NDIR was calibrated using gas standards with air pCO_2 values of 410, 1007 and 5035 ppmv (White Martins Certified Material, RJ, Brazil). For calibration of the gas analyser, fresh soda lime was used to set the zero and the standard at 1007 ppmv to set the span. The air standards at 410 and 5035 ppmv were used to verify the linearity of the response. The accuracy of the pCO_2 measurements is estimated at ±5 ppmv. The partial pressure of atmospheric CO_2 was measured in dry air twice a day, at the start and the end of the continuous measurements.

2.3.2 Discrete parameters

Water samples were filtrated on a glass filtration system through pre-combusted GF/F glass fiber filters (porosity 0.7 μm). One filter was weighed prior to filtration and was then dried for suspended particulate matter (SPM) and particulate organic carbon (POC) determination. SPM was determined gravimetrically on the dried pre-weighed filters. POC content were determined after removing carbonates by adding some drops of HCl 2 N on the filters (Etcheber et al. 2007). The POC analysis was carried on a LECO C-S 125 total carbon analyser based on direct combustion in an induction furnace and infrared absorption determination of the CO_2 produced. Another filter was frozen at -20 °C for further chlorophyll a (Chl *a*) analysis. After extraction in 90% acetone, the Chl *a* was quantified spectrophotometrically before and after acidification of the samples, with formulations and corrections proposed by Strickland and Parsons (1972). Part of the filtrated water was stored in 50 mL, acidified with 100 μL of ultrapure H_3PO_4 and stored in the dark until dissolved organic carbon (DOC) analysis. The DOC analysis was performed with a high temperature catalytic oxidation (HTCO) method using a Shimadzu TOC 500 analyser (Abril et al. 2002). Another part of the filtrate

was stored also in the dark in 150 mL polyethylene flasks for total alkalinity (TA) analysis. TA was titrated with an automated titration system (Metler Toledo model T50) with normalized 0.1 HCl on duplicate 50 mL aliquots and the equivalence point was determined using the linearization of the Gran (1952) function between pH 4 and pH 3. TA measurements were compared to certified reference material (CRM, provided by A. G. Dickson from Scripps Institution of Oceanography) and the accuracy was of ±5 µmol kg^{-1}. River samples were conditioned the same way to analyse POC, DOC during both cruises and also Chl *a* in Feb. 2020.

2.4. Carbonate system and CO_2 fluxes calculations

We used the CO2sys program (Pierrot et al. 2006), version 2.1, to calculate all the chemical species of the carbonate system. The DIC concentrations were calculated from the measured pCO_2 and TA, using the carbonic acid constants sets proposed by Mehrbach et al. (1973) refitted by Dickson and Millero (1987), the borate acidity constant from Lee et al. (2010), and the CO_2 solubility coefficient of Weiss (1974). Considering the analytical accuracies for temperature (0.05°C), TA (±5 µmol kg^{-1}) and pCO_2 (5ppmv) we estimate the error on DIC calculation at ±5 µmol kg^{-1}. The water-atmosphere CO_2 flux (FCO_2) was calculated using the equation, expressed in terms of partial pressure:

$$FCO_2 = k\alpha\Delta pCO_2 \quad (1)$$

where k is the gas transfer velocity of CO_2 (m d^{-1} or cm h^{-1}), α is the solubility coefficient of CO_2 (mol m^{-3} atm^{-1}), and ΔpCO_2 is the air–water gradient of pCO_2 (in atm). The atmospheric pCO_2 data used was 410 ppmv as measured in air during the campaigns. The gas transfer velocity k was calculated from the gas transfer velocity normalized to a Schmidt number of (Jähne et al. 1987):

$$k = k_{600} (600/Sc)^n \quad (2)$$

where k_{600} is the normalized gas transfer velocity, Sc is the Schmidt number of a given gas at a given temperature (Wanninkhof 1992), and n equals 2/3 as in lakes environments (Jähne et al. 1987). To calculate k_{600}, in order to account for the uncertainty on this parameter, we used three different parameterizations respectively noted W92, RC01, and A09: the one of Wanninkhof (1992) representative for the global ocean, and the ones of Raymond and Cole (2001) and Abril et al. (2009), representative for estuarine systems. The three equations are defined as a function of wind speed at 10 meters (U10), and the A09 equation also considers the estuarine surface area and water current velocity. To determine k_{600} we used U10 by the Instituto Nacional de Meteorologia (INMET) at the Sampaio Correia automatic weather station, located ~10 km from Saquarema lagoon (Fig. 1). In the A09 model, we used an average water current set to 20 cm s^{-1} for the Saquarema lagoon and the contribution on k_{600} was less than 8%. The fluxes were computed with the three parameterizations of

k_{600}. However, none of these parameterizations adapt perfectly to hydrographic and morphological features of the Saquarema lagoon; the W92 equation is valid for the open ocean and probably underestimates the k_{600} in the lagoon, whereas the RC01 and A09 equations are valid for funnel-shaped macrotidal estuaries, and probably overestimates the k_{600}. Therefore, we present here the CO_2 fluxes calculated with the three different parameterizations, and the fluxes calculated as the average of the three.

2.5. Statistical analysis

A Kolmogorov-Smirnov test was performed to check the normality of the data and the Levene's test the homoscedasticity of the variances. All statistical analyses were based on $\alpha = 0.05$. When the data showed a normal distribution with equal variances, we used the analysis of variance, ANOVA to examine the seasonal and spatial variation in the parameters. When the data did not follow a normal distribution, we used the Kruskall-Wallis test and, to examine the daytime variation in the parameters, we used the Mann-Whitney test. Correlation analysis between variables was performed with the Spearman rank coefficient. We used the PAST 4.0 program to perform statistical tests.

3 Results

3.1 Spatial and temporal variations of carbon species and ancillary parameters

The two sampling periods were quite contrasted in terms of meteorological and hydrological conditions. The data were compiled according to spatial and temporal samplings and the two sampling periods are presented separately. Table 1 summarizes the average concentrations, and respective standard deviations and ranges, of relevant parameters for this study (T, S, pCO_2, SPM, DOC, POC, Chl *a*, TA and DIC). The most outstanding feature of the two campaigns was the presence of higher salinity and colder waters entering the lagoon during the high tide in Feb. 2020 (Figs. 3 and 4). Upwelling waters with temperatures down to 16 °C and salinities up to 34.47 were observed at the mouth of the Saquarema lagoon in Feb. 2020 while in Nov. 2019 maximum salinity was 30.2 and minimum temperature was 23.5 ºC (Figs. 3 and 5; Table 1). A second important difference between seasons and particularly the spatial surveys was the warmer temperature inside the lagoon in summer in Feb. 2020 (29.56 ± 1.14 º C) compared to spring in Nov. 2019 (24.17 ± 0.77 ºC) (Figs. 2 and 3).

In the Saquarema lagoon the salinity ranged from 14.3 to 34.6 and was strongly correlated with carbonate chemistry parameters, including TA (r = 0.960; Fig. 4 I and 4 J) and DIC (r = 0.925; Fig.

4 K and 4 L). TA decreased from the mouth toward the Mombaça compartment where salinity was the lowest. In salinity 14.3, the TA and DIC concentrations were, for the two cruises, 1466 and 1091 μmol kg^{-1}, respectively. For marine sampled in Feb. 2019 (salinity 34.6) the TA and DIC concentration were respectively 2376 and 2211 μmol kg^{-1} (Fig. 6). Furthermore, both TA and DIC averages were significantly different between the two sampling periods (Mann-Whitney, $p<0.0001$). During both campaigns, pCO_2 showed undersaturated conditions inside the lagoon with a mean of 156 ± 82 ppmv during the spatial survey (Figs. 2 and 3). Surface water pCO_2 decreased with salinity inside the lagoon (Fig. 3). However, in Feb. 2020, the cold marine waters sampled during flood tides at the outlet of the lagoon presented oversaturated pCO_2 values with a mean value of 497 ± 40 ppmv (salinities between 33 and 35). For both spatial and temporal surveys during the two campaigns, DOC, POC and Chl *a* increased inside the lagoon, contrarily to salinity, DIC, TA and pCO_2 (Fig. 4). The minimum concentration of Chl *a* was 2.7 μg L^{-1} at the mouth of the lagoon at high tide and salinity 35 (Fig. 4G and 4H). In the most inner part of the lagoon, in salinities below 15, the concentration of the Chl *a* reached 217 μg L^{-1} (Fig. 4G and 4H). DOC concentrations showed a minimum of 1.0 mg L^{-1} at high salinity (~35) and a maximum of the 19.8 mg L^{-1} values at salinities of ~17 (Fig. 4A and 4B). POC varied between 0.4 mg L^{-1} in seawater entering the lagoon and 12.3 mg L^{-1} in the Mombaça compartment inside the lagoon (Fig. 4C and 4D).

3.2. Spatial variation of pCO_2 in surface waters and CO_2 exchanges at the air-water interface

Inside the lagoon, during both spatial sampling in Nov. 2019 and Feb. 2020, water was undersaturated in CO_2 with respect to the atmosphere and strong spatial gradients occurred between the inner lagoon and its mouth. The lagoon was a sink of CO_2 during the measurements at daytime. For the whole lagoon, an average pCO_2 of 177 ± 73 ppmv was observed in Nov. 2019 and 126 ± 52 ppmv in Feb. 2020. Undersaturated pCO_2 values occurred in the interior of the lagoon with the lowest value down to ~60 ppmv at low salinities. In Fora lagoon close to the outlet to the sea, we observed higher, but still undersaturated pCO_2 values (301 ppmv in Nov. 2019 and 250 ppmv in Feb. 2020). There was significant spatial differences between the measured pCO_2 in the Fora and Mombaça/Jardim compartments (Kruskall-Wallis, $p<0.001$; Table S1). However, we found no significant difference between the Mombaça and Jardim compartments (Kruskall-Wallis, $p>0.05$). The salinity was significantly different between the three compartments in the lagoon (ANOVA, $p<0,001$). In contrast, temperature was not significantly different between compartments (Kruskall-Wallis, $p>0.05$). There was also significant seasonal variability in salinity and temperature (Table S2): inside the lagoon water was significantly warmer in Feb. 2020 compared to Nov. 2019 (ANOVA, $p>0,05$) at the outlet

of the lagoon, the seawater at high tide was cooler and more saline in Feb. 2020 compared to Nov. 2019 (ANOVA, p>0,05).

Wind speed was in general low during the samplings, on average between 2.03 ± 0.9 m s^{-1} and 2.83 ± 0.6 m s^{-1} in Nov. of 2019. In Feb. of 2020, the wind speed average was 2.8 ± 1.0 m s^{-1} in at day time (Table 2). As expected, the k600 values calculated with the equation of Abril et al. (2009) representative for macro-tidal estuaries were higher than those calculated with the relationships of Raymond and Cole (2001) representative for a large variety of estuaries, and of Wanninkhof (1992) representative for the open ocean. Inside the Saquarema lagoon was a sink of atmospheric CO_2 during the two sampled period. Averaged calculated CO_2 fluxes with the three k_{600} parameterizations varied between -2.6 ± 4.8 mmol m^{-2} h^{-1} in Nov. 2019 and -5.6 ± 2.4 mmol m^{-2} h^{-1} in Feb. 2020.

3.3. Tidal variation of pCO_2 in surface waters and CO_2 exchanges at the air-water interface

During the temporal monitoring experiments at the mouth of the lagoon significant variation of salinity, temperature and pCO_2 occurred in summer (Feb. 2020) (Fig. 5; Table 1) but not in spring in Nov. 2019 (Table 1). Maximum water pCO_2 of 524 ppmv was observed at high tide (Table 1, Fig. 3), with corresponding temperature of 16.3 °C and a salinity of 34.4. At the same sampling point but at low tide, water pCO_2 was 194 ppmv for temperature of 28.16 °C and a salinity of 28.36, showing simultaneous warming and mixing with brackish waters, and biological uptake of CO_2. The pCO_2 was not significantly different between day and night (p >0.05 Mann–Whitney test), but it was between ebb and flood tides. Calculated CO_2 fluxes were -2.7 ± 0.5 mmol m^{-2} h^{-1} in Nov. 2019. In Feb. 2020 the CO_2 fluxes average varied between -4.6 ± 1.8 mmol m^{-2} h^{-1} in the ebb tide and +0.8 ± 2.1 mmol m^{-2} h^{-1} at the mouth of the lagoon during the intrusion of upwelling waters with flood tides.

4. Discussion

4.1. Mixing between lagoon and ocean waters as drivers of air-sea CO_2 fluxes

The contrasting climatic conditions between the two surveys were reflected by the distribution of the salinity gradient in the lagoon, as well as the carbonate species, particularly pCO_2. In Nov. 2019, we

could not observe an entrance of pure oceanic water during the 12h measurements. Highest salinity at the mouth of the lagoon at high tide was only 30.2 (Table 1) at that season, when, in addition, the Cabo Frio Upwelling is not active (Coelho-Souza et al. 2012). The monitoring in Nov. 2019 occurred during particularly bad meteorological conditions, with strong S-SW winds the day before sampling. Such conditions generally promote a large entrance of shelf water in the lagoon (Oliveira 2013); however, this was not clear during our monitoring, even at high tide (see Table 1). Because salinity remained lower than pure seawater salinity, this water contained a significant fraction of CO_2-depleted water from the lagoon and pCO_2 values remained undersaturated as those inside the lagoon, at about 300 ppmv and salinities up to 31.9 (Fig. 3; Table 1). In contrast, in Feb. 2020, the marine end-member was very marked, with colder and more saline waters, supersaturated in CO_2. At that season the Cabo Frio upwelling was at maximum intensity (Coelho-Souza et al. 2012), and throughout the entire flood tides, the cold SACW with a pCO_2 of 520 ppmv entered the lagoon (Fig. 5). The well-defined temperature and pCO_2 gradients between the lagoon and the ocean in Feb. 2020 allow a detailed quantitative analysis of carbonate thermodynamics during the mixing of two end-members: the first one is located inside the lagoon at salinity 10 and the second one is the SACW sampled during flood tides at the mouth of the lagoon at salinity ~ 35.

Inside the lagoon, our continuous measurements in Feb. 2020 went down to salinity 10 (Fig. 3), whereas the less saline discrete sample for TA analysis had a salinity of 14.3 (Fig. 4). We could extrapolate the strong linear correlation between TA and salinity (Fig. 4L) to estimate TA at salinity 10. In the salinity range 0 to 10 that occurs at the outlet of several small rivers, changes were too abrupt to allow precise surface water sampling, in addition to being very shallow, making it impossible to travel with the boat. According to previous works on the hydrology of the Saquarema lagoon (Alves 2013), the mixing between lagoon and seawater during the field campaigns occurred at two different timescale: the mixing between salinity 35 and 29 occurs in the Fora compartment on a short timescale, related to the tide; the mixing between salinity 29 and 10 occurs all the compartments until the Mombaça compartment (Fig. 1) on much a longer time scale (56-58 days; Alves 2013). From the TA and pCO_2 values in these two end-members, we calculate the DIC values and we established the equations of the conservative mixing lines for temperature, TA and DIC as a function of salinity as follows:

$$TA_{cons}(S) = TA(10) + (S - 10).\frac{TA(35) - TA(10)}{35 - 10}$$

$$DIC_{cons}(S) = DIC(10) + (S - 10).\frac{DIC(35) - DIC(10)}{35 - 10}$$

$$T_{cons}(S) = T(10) + (S - 10).\frac{T(35) - T(10)}{35 - 10}$$

Where TA_{cons} (S), DIC_{conc} (S) and T_{cons} (T) are respectively the TA, DIC and T at salinity S resulting from the conservative mixing of the two end-members. Then, from these three parameters, we calculated the theoretical pCO_2(S) resulting from conservative mixing of the two end-members by solving the carbonate system for each 0.5 salinity increments between 10 and 35, (Jiang et al. 2008; Joesoef et al. 2015; Cotovicz et al. 2020; Abril et al. 2021). This led to a first theoretical conservative pCO_2 mixing curve (Fig. 6). We also evaluate the theoretical impact of water heating on pCO_2. To do this, we performed the same pCO_2 calculation for each 0.5 salinity interval, using, this time, the *in situ* measured temperature, TA_{cons}(S) and DIC_{cons} (S). Finally, we have binned our measured data for 0.5 salinity intervals between 10 and 35 to allow a quantitative comparison between the observed pCO_2 and the two modelled pCO_2.

Results of this analysis are shown in Fig. 6 and reveal that in Feb. 2020, when the cold SACW supersaturated in CO_2 starts mixing with the lagoon waters at the tidal time scale in the Fora compartment, it simultaneously undergoes important heating that should potentially increase the pCO_2 until a maximum value of 580ppmv at salinity 29. At salinities lower than 29, the mixing with undersaturated lagoon water would make the pCO_2 decrease until salinity 10. The pCO_2 field measurements do not follow the trend predicted by the mixing model, revealing the occurrence of strong biological uptake of CO_2 within the lagoon. At the tidal timescale, from salinity 35 to 29, although heating should in theory increase pCO_2 by about 60ppmv, the observed pCO_2 rapidly drops from 520 to 190 ppmv. Between salinities 29 and 10, on a timescale longer than a month, the pCO_2 continues to decrease remaining below the theoretical conservative mixing line (Fig. 6), within the range 80-200ppmv, and similar to the situation in Nov. 2019 (Fig. 3C). The mixing model in Feb. 2020 indicates that in the Fora compartment, the biological uptake of CO_2 by the planktonic autotrophic community was efficient enough to absorb the excess CO_2 carried by upwelling waters, plus the one resulting from the heating of the oceanic cold waters, making the lagoon to act as a net CO_2 sink. This situation in Saquarema lagoon during the intrusion of upwelling waters, contrasts with the one in a Baja California coastal lagoon in Mexico, where CO_2 outgassing prevails particularly during the periods of upwelling (Ribas-Ribas et al. 2011; Ávila-López et al. 2016). In the Aby and Tendo lagoons in Ivory Coast, a CO_2 sink has also been reported, although it was related to a

thermohaline stratification of the water column (Koné et al. 2008). Despite its specific hydrological settings, the Saquarema Lagoon acts as a CO_2 sink similarly to the neighbouring Guanabara Bay and Araruama hypersaline lagoon (Cotovicz et al. 2016; 2021), with phytoplankton productivity acting as the major driver on CO_2 air-sea fluxes.

Another interesting fact revealed by our study is the relative stability between the two surveys of the low pCO_2 values in the most confined waters of the lagoon, in the Jardim and Mombaça compartments where water residence time is longer (Table 1; Fig. 2). Seasonally, the average daytime pCO_2 inside the lagoon was significantly lower (Mann-Whitney, p>0,001; Table S2) in Feb. 2020 (126 ± 52 ppmv) than in Nov. 2019 (177 ± 73 ppmv) (Fig. 2; Table 1). During the spatial surveys, waters were about 5°C cooler in Nov. 2019 compared to Feb. 2020, which corresponds to a theoretical thermal pCO_2 increase of about 7 ppmv, instead of the observed decrease of about 51 ppmv. In Feb. 2020 the Chl *a* concentrations were significantly (Mann-Whitney, p<0,001) higher than in Nov. 2019 (Fig. 4), revealing that the modest seasonal pCO_2 changes inside the lagoon was associated to enhanced phytoplankton production in Feb. 2020. Feb. 2020 was characterized by denser phytoplankton blooms, apparently adapted to rapidly absorb large quantities of CO_2 diffusing from the atmosphere as well as all the dissolved CO_2 brought with the SACW at that season. In contrast to the average values, the lowest pCO_2 values were identical at both seasons at 60ppmv (Fig. 3; Table 1). These pCO_2 minima were observed in the 15-25 salinity range around midday, before thermal winds start to blow. This apparent constant threshold value for CO_2 consumption in the lagoon waters may be due to a combination of various factors including surface heating and transient stratification, nutrient and/or CO_2 limitation in the photic layer, photo-inhibition of phytoplankton species, including eukaryotes and cyanobacteria (Caraco and Miller 1998; Phlips et al. 2002), as well as higher re-aeration rates at very low pCO_2.

4.2. Links between inorganic and organic carbon

In addition to the clear spatial and temporal negative correlations between pCO_2 and phytoplanktonic biomass (Fig. 7), the links between inorganic and organic carbon is a crucial point in order to explain the drivers of the CO_2 sinks in the Saquarema lagoon. During the 25h cycle at the mouth of the lagoon in Feb. 2020, the POC and DOC expressed as mg L^{-1}, the POC% and the SPM concentrations varied all together (Fig. 5). Lagoon waters flowing to the ocean during the ebb tides had much greater concentrations of DOC, POC and SPM and their SPM were enriched in POC, compared to the SACW entering during the flood tides. Consequently, the lagoon behaved as a source of POC and DOC for

411 the offshore marine waters. When considering the entire dataset (spatial and temporal monitoring), a
412 negative correlation is observed between DIC and Total Organic Carbon (TOC) (Fig. 9). The SACW
413 have the highest pCO_2, highest DIC and lower TOC concentrations, whereas the less saline samples
414 inside the Monbaça and Jardim compartments have lower pCO_2 and DIC and higher TOC. However,
415 the slope -2.3±0.1 of the correlation in fig. 9 reveals that the landward DIC decrease is only about
416 half of the landward TOC increase. At the outlet of the lagoon in Feb. 2020, the TOC concentrations
417 during ebb tides were 11.8±4.6 mgC L^{-1} higher than those during flood tides, whereas the DIC
418 concentrations during ebb tide were only 5.1 ± 2.7 mgC L^{-1} lower than those during flood tide. The
419 exchanges between the lagoon and the ocean can be estimated thanks to the average tidal prim in the
420 lagoon, estimated from a modelling work to 1.4 10^6 m^3 on average (Oliveira 2013). Using this tidal
421 prism and the differences in carbon concentration between ebb and flood in Feb. 2020 (Fig. 5), we
422 calculate exports from the lagoon of 21 tC d^{-1} of DOC and 14 tC d^{-1} of POC and an import of only 15
423 tC d^{-1} of DIC. The penetration of atmospheric CO_2 through the air-lagoon interface (Table 2) provided
424 an additional 1.4 tC d^{-1} of DIC in Feb. 2020 (0.8 tC d^{-1} of DIC in Nov. 2019). Although they are very
425 rough estimates, these fluxes suggest first, that the carbon flux at the air-lagoon interface is one order
426 of magnitude lower than the tidal exchange of DIC with the ocean, and second, that the lagoon exports
427 more than twice as much TOC than it imports DIC. Consequently, if phytoplankton converts DIC to
428 TOC with a 1:1 ratio, an additional source of TOC would be necessary to balance the carbon budget
429 of the lagoon.
430
431 Several processes can potentially contribute to this disequilibrium between inorganic and organic
432 carbon along the salinity gradient: (1) dilution of DIC and import of TOC with freshwater; (2)
433 phytoplankton production that consumes DIC and produces POC and eventually DOC; (3) gas
434 exchange and invasion of atmospheric CO_2 that will contribute to DIC; (4) other sources of POC and
435 DOC occurring in the most confined waters of the lagoon, where waters are CO_2-depleted. Estuarine
436 DOC and POC can have three origins: terrestrial, marine and estuarine primary production (Abril et
437 al. 2002; Bauer et al. 2013). In the case of the Saquarema lagoon, wastewater carried by small rivers
438 and flowing from multiple point sources all around the lagoon, is also an additional potential source
439 of POC and DOC (Carmouze et al. 1991).
440
441 The impact of mixing of the lagoon waters with freshwater is more difficult to evaluate quantitatively
442 because our river data are partial due to logistical constrains, because sampling in many more small
443 rivers as well as hydrological data would be necessary, and because the distribution of the carbon
444 species in the 0-10 salinity range was inaccessible. The significant seasonal increase in POC and DOC

concentrations in the rivers and inside the lagoon (Fig. 4) as well as the lower salinity in the lagoon (Table 1) in Feb. 2020, suggest that rivers could deliver more POC and DOC during the rainy summer. However, this season is also warmer and more productive for phytoplankton as attested by the higher Chl *a* concentration and the lower pCO_2. At the river stations, DOC and POC concentrations were higher than in seawater, but lower than in the Mombaça inner compartment of the lagoon at salinity between 15 and 20 where Chl *a* concentrations are maximal at both seasons (Fig. 4), suggesting also the presence of phytoplankton-derived POC and DOC. POC:Chl *a* ratios indicate very different contributions of phytoplankton biomass to the POC in the three sampled rivers, in the inner lagoon and at the mouth, and in the SACW (Fig. 8). In all the Feb. 2020 samples, and half of the Nov. 2019 samples in the Mombaça and Jardim compartments, as well as in the SACW samples, this ratio was within the range of 15 and 140 which corresponds to a predominant contribution of living phytoplankton to the POC (Cloern 1996; Abril et al. 2002; Sathyendranath et al. 2009; Cloern et al. 2014). In river samples, the ratio was much higher (Fig 8), which confirms a terrestrial and/or domestic origin of POC (Abril et al. 2002).

Concerning DOC, the facts that concentrations inside the lagoon were highest in summer and were higher than in the river and ocean end-members at both seasons (Fig. 4) indicate an internal source that can be multiple sewage point sources and phytoplankton exudation or lysis. On one occasion, high DOC was also observed in the most polluted river with a maximum value in February, when runoff was apparently higher than in November. The distributions of DOC along the salinity gradient indicate a net production inside or input into the lagoon at both seasons, as well as a close to conservative dilution in the 15-35 salinity range during the mixing of lagoon waters with seawater (Fig. 4). One interesting observation comes from the positive correlation between DOC and Chl *a* and the negative correlation between DOC and pCO_2 (Fig. 7). The same observation was made in the most eutrophic waters of the Guanabara Bay (Cotovicz et al. 2018) suggests that part of DOC comes from the exudation or lysis of microalgae, a common process in coastal waters (Myklestad 2000; Augusti and Duarte 2013). It is interesting to note that both in the Guanabara Bay and in the Saquarema lagoon, DOC concentrations consistently increased to values above 10 mg L^{-1}, when pCO_2 was below 200 ppmv (Fig. 7; Cotovicz et al. 2018), thus, when CO_2 limitation of phytoplankton can occur, together with a strong depletion of inorganic nutrients in the surface water (Lui et al. 2017). This could be due to changes in the composition and physiological state of the planktonic microbial community induced by a combination between physicochemical, biological, climatic and hydrographic factors, in these two urbanized coastal environments.

4.3. Impact of eutrophication on the carbon cycle of the Saquarema Lagoon

Cultural eutrophication of coastal ecosystems is a secular trend in many developing countries, and particularly in the densely populated state of Rio de Janeiro in Brazil (Knoppers and Kjerfve 1999). Eutrophication is due to massive anthropogenic inputs of organic (mainly domestic) and, to a lesser extent, inorganic (agricultural or industrial) nutrients that enrich estuarine waters and sediments with bioavailable nitrogen and phosphorus (Rabalais et al. 2009). In addition, in the case of shallow lagoons, the frequent resuspension of sediments caused by tidal exchange and winds, becomes an important internal source of recycled nutrients, making the lagoons and bays in the region extremely productive (Carmouze et al. 1991). Because of the transparency of their waters, tropical lagoons are recognized as naturally autotrophic ecosystems and eutrophication will enhance this ecosystem property, making them more productive (Carmouze et al. 1991; Knoppers and Kjerfve 1999). Nutrient accumulation in coastal bays and lagoons leads to massive algal blooms, to a general increase of water turbidity, a reduction of light at the bottom, and the progressive loss of native submerged aquatic vegetation and biofilms (Carmouze and Vasconcelos 1992). Our study reveals a CO_2 sink that can be in part explained by eutrophication that enhances autotrophy more than heterotrophy, as reported in diverse coastal ecosystems (*e.g.* Gypens et al. 2009), and as attested by the very high Chl *a* concentrations (Fig. 4GH; Table 1).

In the Saquarema lagoon, inorganic nutrients concentrations remain relatively stable since the 90's with dissolved inorganic nitrogen (DIN) around 5-20 µmol L^{-1} and dissolved inorganic phosphorus around 0,5-1 µmol L^{-1} (Carmouze and Vasconcelos 1992; Carloni et al. 2010). However, inorganic nutrients concentrations are not relevant indices of eutrophication because most of the nitrogen and phosphorus are present in the organic form, which is rarely analysed. Indeed, if the POC concentration is 8 mg L^{-1} (Table 1), and if we assume a C/N Redfield ratio of 10, then the particulate organic nitrogen concentration would be 70 mg L-1, that is 2.5-10 times the DIN concentration. Some previous works in Saquarema have documented Chl *a*, POC and DOC concentrations in the 80's and 90's in the Jardim and Fora compartments (Pereira 1991; Table 3). Although these data are occasional and not fully representative of spatial and seasonal variations in the lagoon, they suggest a decadal increase of these three parameters, as well as a decrease of the POC:Chl *a* ratio, and thus, an increase of the stock of phytoplankton-derived organic carbon with time, particularly in the Jardim compartment (Table 3). Indeed, the most inner compartments of the lagoon have longer water residence times, shallower depths, making them more adapted to the long-term accumulation of nutrients in waters and sediments and enhanced planktonic primary production. In present days, the conditions that create

513 the CO_2 sink in the inner compartments of the Saquarema lagoon appear relatively stable between the
514 two campaigns (see 4.1).
515
516 If we compare with other densely populated tropical and sub-tropical regions, the inner part of the
517 Saquarema lagoon was a sink of atmospheric CO_2 ranging from -5.6 to -2.6 mmol C m^{-2} h^{-1} (Table
518 2), similar to those reported the Guanabara Bay (-7.7 to -3.53 mmol C m^{-2} h^{-1}; Cotovicz et al. 2015)
519 and higher than those reported in the Araruama hypersaline lagoon (-0.2 to -0.6 mmol C m^{-2} h^{-1};
520 Cotovicz et al. 2021), in the Aby Lagoon in Ivory Coast (-0.3 mmol C m^{-2} h^{-1}; Koné et al. 2009) and
521 in Tokyo Bay (-0.4 mmol C m^{-2} h^{-1}; Kubo et al. 2017). The mechanism of carbon cycling in coastal
522 environments impacted by urban pollution has been discussed by Kubo et al. (2017) as the balance
523 between the more active respiration due to the presence of sewage derived organic matter and the
524 more active photosynthesis driven by nutrient accumulation. This leads to a border between nearshore
525 waters close to the sewage outlet that act as CO_2 sources because degradation of organic matter locally
526 predominates and offshore waters that act as CO_2 sink because phytoplankton production overwhelms
527 the CO_2 budget. Cultural eutrophication apparently tends to shift this border toward the landside
528 (Kubo et al. 2017). In Tokyo Bay, implementation of sewage treatments since the 70's have reduced
529 the loads of biodegradable organic carbon but not the loads of nutrients; as a result, the respiration
530 was reduced but the phytoplanktonic production was favoured, and the Tokyo Bay acts as a strong
531 CO_2 sink (Kubo and Kanda 2020). In Guanabara and Tokyo bays, and in Araruama lagoon, the
532 sewage loads are concentrated to well identified regions that emit CO_2 to the atmosphere but represent
533 a limited surface area (Cotovicz et al. 2015; 2021; Kubo et al. 2017). In the Saquarema lagoon, the
534 CO_2 supersaturation of water was linked to the intrusion of SACW in Feb. 2020 that acted as a weak
535 source of CO_2, of 0.2±0.3mmol C m^{-2} h^{-1}, for *k*W92, well within the range reported in the continental
536 shelf of the subtropical Atlantic Ocean (ranging from 0.01 to 0.4 mmol C m^{-2} h^{-1}, Ito et al. 2016).
537 CO_2 supersaturation did not occur in the inner compartments where domestic carbon and nutrient are
538 carried by rivers but also from multiple point sources all around the lagoon (Carloni et al. 2010). This
539 suggests that, even if degradation of organic matter derived from sewage is probably occurring, in the
540 environmental conditions of the lagoon, it cannot outcompete with the high phytoplanktonic
541 productivity that creates the CO_2 sink. In addition, the TOC export to the ocean was larger than the
542 DIC import (see 4.2) which suggests that this flux included organic carbon originating from sewage.
543
544 Despite the large differences in water depth and residence time, eutrophication has turned the
545 Saquarema lagoon to a CO_2 sink, similarly to the Guanabara Bay (Cotovicz et al. 2015), the Tokyo
546 Bay (Kubo et al. 2017), and the hypersaline Arararuama Lagoon. If the CO_2 fluxes were very similar

in all these systems, the fluxes of POC and DOC are probably very different. One important issue to be investigated in the next future is the fate of the organic C present in these environments: the POC and DOC that is not remineralized is partially exported to the ocean, and partially stored in the sediments. In Guanabara Bay, Cotovicz et al (2015) have emphasized that the air-water CO2 flux was quantitatively similar to the recent organic C burial in the sediments (Carreira et al. 2002). No carbon burial data are available in the Saquarema lagoon. However, recent works in the neighbouring Itaipu lagoon indicate an important increase of organic matter storage in the sediment linked to eutrophication (Cerda et al. 2016). More hydrological and sedimentological data would be necessary in order to quantitatively compare the CO_2 sink with carbon burial and export. In the sea, this organic material may undergo partial degradation and only more refractory compounds would persist longer times in oceanic water masses.

5. Conclusions

The Saquarema lagoon behaved as CO_2 sink during the two sampling surveys. Although the sampling periods are probably not fully representative of the temporal variation, the similar values of pCO_2, POC, DOC and Chl *a* reveal a relative stability of the autotrophic character of the inner compartments of the lagoon. Important contrasts were observed at the mouth of the lagoon between seasons, with the entrance of SACW in Feb. 2020. The response of the lagoon carbonate system to the intrusion of the cold SACW supersaturated in CO_2 was dominated by biological uptake, pCO_2 showing a strong non-conservative behaviour during the mixing of seawater with lagoon waters. The negative correlation for both surveys between Chl *a*, POC, DOC on the one hand and pCO_2 and DIC on the other hand reveal that phytoplankton inside the lagoon was very efficient at converting inorganic carbon to both particulate and dissolved organic carbon. Our analysis also suggests the TOC exported to the ocean apparently come partly from sewage sources and partly from phytoplankton production inside the lagoon. Our study confirms that intense eutrophication of tropical semi-enclosed littoral ecosystems, including bays and lagoons, turns these surface waters to act as CO_2 sinks and accumulators and exporters of organic carbon.

Acknowledgments

This research was funded by the Fundo Brasileiro para a Biodiversidade (FUNBIO) project: "*Mecanismos Reguladores da Produção Pesqueira nos Sistemas Lagunares do Leste Fluminense: estado atual e cenários futuros*" and the France-Brazil International Research Project VELITROP (*Vulnérabilité des Ecosystèmes Littoraux Tropicaux face à l'Eutrophisation*) funded by the French National Centre for Scientific Research (CNRS-INEE). We thank Leandro Alves, Mauricio Lorenzo Cerda Lema, Francisco Fernando Lamego Simões Filho, and Tailan Moretti Mattos from the Aquatic Biogeochemitry Lab. at the Universidade Federal Fluminense for their valuable help in the field.

References

Abril, G., Libardoni, B.G., Brandini, N., Cotovicz, L.C.Jr, Medeiros, P.R.P., Cavalcante, G.H., Knoppers, B.A., 2021. Thermodynamic uptake of atmospheric CO_2 in the oligotrophic and semiarid São Francisco estuary (NE Brazil). Marine Chemistry 233: 103983.

Abril, G., Nogueira, E., Etcheber, H., Cabeçadas, G., Lemaire, E., Brogueira, M., 2002. Behaviour of organic carbon in nine contrasting European estuaries. Estuar Coast Shelf Sci 54:241–262.

Abril G., Commarieu M.V., Sottolichio, A., Bretel, P., Guérin, F., 2009. Turbidity limits gas exchange in a large macrotidal estuary. Estuar. Coast. Shelf Sci. 83, 342–348.

Abril, G., Richard, S., Guérin, F., 2006. In-situ measurements of dissolved gases (CH_4 and CO_2) in a wide range of concentrations in a tropical reservoir using an equilibrator, Sci. Total Environ, 354, 246–251.

Augusti, S. and Duarte, C.M., 2013. Phytoplankton lysis predicts dissolved organic carbon release in marine plankton communities. Biogeosciences 10:1259–1264. https://doi.org/ 10.5194/bg-10-1259-2013

Ávila-López, M.C., Hernández-Ayón, J.M., Camacho-Ibar ,V.F., Bermúdez, A.F., Mejía-Trejo, A. Pacheco-Ruiz, I., 2016. Air–Water CO_2 Fluxes and Net Ecosystem Production Changes in a Baja California Coastal Lagoon During the Anomalous North Pacific Warm Condition. Estuaries and Coasts doi.10.1007/s12237-016-0178-x

Alves, A.R., 2003. Modelagem numérica como ferramenta de gestão ambiental. Aplicação ao sistema lagunar de Saquarema, RJ. Dissertação de Mestrado, Universidade Federal Fluminense, 97 p.

611 Bauer, J.E., Cai, W.-J., Raymond, P., Bianchi, T.S., Hopkinson, C.S., Regnier, P.G., 2013. The
612 changing carbon cycle of the coastal ocean. Nature 504, 61–70.
613 https://doi.org/10.1038/nature12857.
614 Borges, A.V. and Abril, G., 2011. Carbon dioxide and methane dynamics in estuaries, in: Treatise on
615 Estuarine and Coastal Science, edited by: Eric, W. and Donald, M., Academic Press,
616 Amsterdam, 119–161
617 Borges, A.V., 2005. Do We Have Enough Pieces of the Jigsaw to Integrate CO_2 Fluxes in the Coastal
618 Ocean? Estuaries, v. 28, n. 1, p. 3–27.
619 Borges, A.V., Delille, B., Frankignoulle, M., 2005. Budgeting sinks and sources of CO_2 in the coastal
620 ocean: Diversity of ecosystems counts. Geophysical Research Letters, v. 32, n. 14, GL023053.
621 Cai, W-J., Dai, M., Wang, Y., 2006. Air-sea exchange of carbon dioxide in ocean margins: a province-
622 based synthesis. Geophys. Res. Lett. 33:L12603.
623 Cai, W.J., 2011. Estuarine and coastal ocean carbon paradox: CO_2 sinks or sites of terrestrial carbon
624 incineration? Ann. Rev. Mar. Sci. 3, 123–145.
625 Caraco, N., and Miller, R., 1998. Direct and indirect effects of CO_2 on competition between
626 cyanobacteria and eukaryotic phytoplankton, Canadian Journal of Fisheries and Aquatic
627 Sciences, n. 55, pp. 54-62.
628 Carloni, F.B.B.A., 2010. Mudanças na qualidade da água de uma laguna do leste fluminense, geradas
629 pela abertura permanente de conexão com o mar. Geochimica Brasiliensis. V. 24, n.
630 Geochimica Brasiliensis 1, p. 29 – 40.
631 Carmouze, J.P. and Vasconcelos, P., 1992. The eutrophication of the Lagoon of Saquarema, Brazil.
632 Science of Total Environment, v.Supplement, p.851-859.
633 Carmouze, J., Knoppers, B.A., Vasconcelos, P.A., 1991. Metabolism of Saquarema Lagoon, Brazil.
634 Biogeochemistry, v. 2.
635 Carreira, R.S., Wagener, A.L.R., Readman, J.W., Fileman, T.W., Macko, S.A., Veiga, Á., 2002.
636 Changes in the sedimentary organic carbon pool of a fertilized tropical estuary, Guanabara Bay,
637 Brazil: an elemental, isotopic and molecular marker approach, Mar. Chem., 79(3-4), 207–227,
638 doi:10.1016/S0304-4203(02)00065-8.
639 Castelão, R.M. and Barth, J.A., 2006. Upwelling around Cabo Frio, Brazil: The importance of wind
640 stress curl. Geophys. Res. Lett 33(3), doi.org/10.1029/2005GL025182.
641 Cerda, M., Barboza, C.D.N., Carvalho, C.N.S.; Jandre, K.A., Marques Jr, A.N., 2013. Nutrient
642 budgets in the Piratininga-Itaipu lagoon system (southeastern Brazil): effects of sea-exchange
643 management. Proceedings of the 3rd Brazilian Congress of Marine Biology. Lat. Am. J. Aquat.
644 Res., 41(2): 226-238.

Cerda, M., Scali, C., Valde, J., Macario, K.D., Anjos, R.M., Vogel, V., Lamego, F., Nepomuceno, A., 2016. Coupling fallout 210Pb and stables isotopes (δ13C, δ15N) for catchment urbanization reconstruction in southeastern coastal zone of Brazil. J. Radioanal. Nucl. Chem. 310, 1021–1032.

Chen, C.T.A. and Borges, A.V., 2009. Reconciling opposing views on carbon cycling in the coastal ocean: Continental shelves as sinks and near-shore ecosystems as sources of atmospheric CO_2, Deep-Sea Res., v. 56, p. 578–590.

Chen, C.-T.A., Huang, T.-H., Chen, Y.-C., Bai, Y., He, X., Kang, Y., 2013. Air–sea exchanges of CO_2 in the world's coastal seas. Biogeosciences 10, 6509–6544. https://doi.org/10.5194/bg-10-6509-2013.

Cloern, J.E., Foster, S.Q., Kleckner, A.E., 2014. Phytoplankton primary production in the world's estuarine-coastal ecosystems. Biogeosciences, v. 11, p. 2477–2501.

Cloern, J.E., 1996. Phytoplankton bloom dynamics in coastal ecosystems: a review with some general lessons from sustained investigation of San Francisco Bay, California. Rev. Geophys. 2, 127–168. https://doi.org/10.1029/96RG00986.

Coelho-Souza, S.A., López, M.S., Guimarães, J.R.D., Coutinho, R., Candella, R.N., 2012. Biophysical interactions in the Cabo Frio upwelling system, Southeastern Brazil. Brazilian J. Oceanogr. 60, 353–365. https://doi.org/10.1590/S1679-87592012000300008.

Cotovicz, Jr. L.C., Knoppers, B.A., Régis, C.R.; Tremmel, D., Costa-Santos, S., Abril, G., 2021. Eutrophication overcoming carbonate precipitation in a tropical hypersaline coastal lagoon acting as a CO_2 sink (Araruama Lagoon, SE Brazil). Biogeochemistry doi.org/10.1007/s10533-021-00842-3.

Cotovicz Jr, L., Vidal, L., Rezende, C., Bernardes, M., Knoppers, B., Sobrinho, R., Cardoso, R., Muniz, M., dos Anjos, R., Biehler, A., Abril, G., 2020. Sources and sinks of CO_2 in the delta of the Paraíba do Sul River (Southeastern Brazil) modulated by carbonate thermodynamics, gas exchange and ecosystem metabolism during estuarine mixing. Marine Chemistry. 103869. 10.1016/j.marchem.2020.103869.

Cotovicz Jr, L.C., Knoppers, B.A., Brandini, N., Poirier, D., Costa Santos, S.J., Cordeiro, R.C., Abril, G., 2018. Predominance of phytoplankton-derived dissolved and particulate organic carbon in a highly eutrophic tropical coastal embayment (Guanabara Bay, Rio de Janeiro, Brazil). Biogeochemistry, 137, 1–14.

Cotovicz Jr, L.C., Knoppers, B. A., Brandini, N., Costa Santos, S.J., Abril, G., 2015. A strong CO_2 sink enhanced by eutrophication in a tropical coastal embayment (Guanabara Bay, Rio de Janeiro, Brazil). Biogeosciences 12, 6125–6146.

679 Cotovicz Jr, L.C., Libardoni, B., Brandini, N., Knoppers, B., Abril, G., 2016. Comparações entre
680 medições em tempo real da pCO_2 aquática com estimativas indiretas em dois estuárioss
681 tropicais contrastantes: o estuário eutrofizado da Baia de Guanabara (RJ) e o estuário
682 oligotrofico do Rio São Francisco (AL). Quím. Nova 39, 1206–1214.
683 Dickson, A.G. and Millero, F.J., 1987. A comparison of the equilibrium constants for the dissociation
684 of carbonic acid in seawater media, Deep-Sea Res., 34, 1733–1743.
685 Etcheber, H., Taillez, A., Abril, G., Garnier, J., Servais, P., Moatar, F., Commarieu M.-V., 2007.
686 Particulate organic carbon in the estuarine turbidity maxima of the Gironde, Loire and Seine
687 estuaries: origin and lability. Hydrobiologia 588:245–259.
688 Frankignoulle, M., Abril, G., Borges, A., Bourge, I., Canon, C., Delille, B., Libert, E., Theate, J.M.,
689 1998. Carbon dioxide emission from European estuaries. Science 282, 434–436.
690 https://doi.org/10.1126/science.282.5388.434.
691 Frankignoulle, M., Borges, A., Biondo, R., 2001. A new design of equilibrator to monitor carbon
692 dioxide in highly dynamic and turbid environments, Water Res., 35, 344 – 7.
693 Gattuso, J.-P., Frankignoulle, M., Wollast, R., 1998. Carbon and Carbonate Metabolism in Coastal
694 Aquatic Ecosystems. Annual Review of Ecology and Systematics, v. 29, n. 1, p. 405–434.
695 Gran, G., 1952. Determination of the equivalence point in potentiometric titrations. Part II. The
696 Analyst, v. 77, n. 920, p. 661.
697 Gypens, N., Borges, A.V., Lancelot, C., 2009. Effect of eutrophication on air-sea CO_2 fluxes in the
698 coastal Southern North Sea: a model study of the past 50 years. Global Change Biology 15 (4):
699 1040-1056. 10.1111/j.1365-2486.2008.01773.x.
700 IBGE, 2020. Pesquisa nacional de saneamento básico 2017: abastecimento de água e esgotamento
701 sanitário / IBGE, Coordenação de População e Indicadores Sociais. – Rio de Janeiro: Instituto
702 Brasileiro de Geografia e Estatística.
703 Ito, R.G., Garcia, C.A.E., Virginia, M., 2016. Net sea-air CO_2 fluxes and modelled pCO_2 in the
704 southwestern subtropical Atlantic continental shelf during spring 2010 and summer 2011.
705 Continental Shelf Research 119, 68-84. doi: 10.1016/j.csr.2016.03.013.
706 Jähne, B., Munnich, K.O., Bosinger, R., Dutzi, A., Huber, W., Libner, P., 1987. On parameters
707 influencing air-water exchange. J. Geophys. Res. 92, 1937–1949.
708 https://doi.org/10.1029/JC092iC02p01937.
709 Jiang, L.-Q., Cai, W.-J., Wang, Y., 2008. A comparative study of carbon dioxide degassing in river-
710 and marine-dominated estuaries. Limnol. Oceanogr. 53, 2603–2615.
711 doi.org/10.4319/lo.2008.53.6.2603.

712 Joesoef, A., Huang, W.-J., Gao, Y., Cai, W.-J., 2015. Air–water fluxes and sources of carbon dioxide
713 in the Delaware estuary: spatial and seasonal variability. Biogeosciences 12, 6085–6101.
714 https://doi.org/10.5194/bg-12-6085-2015.
715 Knoppers, B.A., Carmouze, J.P., Moreira-Turcqo, P.F., 1999. Nutrient dynamics, metabolism and
716 eutrophication of lagoons along the east Fluminense coast, state of Rio de Janeiro, Brazil. In:
717 Knoppers, B.A., Bidone, E.D., Abrão, J.J. (Eds.). Environmental geochemistry of coastal
718 lagoon systems of Rio de Janeiro, Brazil. Rio de Janeiro: FINEP. p. 123–154.
719 Knoppers, B. and Kjerfve, B., 1999. Coastal lagoons of southeastern Brazil: physical and
720 biogeochemical characteristics. In Estuaries of South America. Springer Berlin Heidelberg. 35-
721 66.
722 Koné, Y.J.M., Abril, G., Kouadio, K.N., Delille, B., Borges, A.V., 2008. Seasonal variability of
723 carbon dioxide in the Rivers and lagoons of Ivory Coast (West Africa). Estuar. Coasts 32, 246–
724 260. https://doi.org/10.1007/s12237-008-9121-0.
725 Körtzinger, A., 2003. A significant CO_2 sink in the tropical Atlantic Ocean associated with the
726 Amazon river plume. Geophys. Res. Lett. 30, 2287, doi:10.1029/2003GL018841.
727 Kubo, A., Maeda, Y., Kanda, J., 2017. A significant net sink for CO_2 in Tokyo Bay. Sci Rep 7:44355.
728 https://doi.org/10.1038/srep44355.
729 Kubo, A. and Kanda, J., 2020. Coastal urbanization alters carbon cycling in Tokyo Bay. Sci Rep 10,
730 20413. https://doi.org/10.1038/s41598-020-77385-4.
731 Lee, K., Kim, T.W., Byrne, R.H., Millero, F.J., Feely, R.A., Liu, Y.M., 2010. The universal ratio of
732 boron to chlorinity for the North Pacific and North Atlantic oceans, Geochim. Cosmochim. Ac.,
733 74, 1801–1811, doi:10.1016/j.gca.2009.12.027.
734 Liu, X., Li, Y., Wu, Y., Huang, B., Dai, M., Fu, F., Hutchins, D.A., Gao, K., 2017. Effects of elevated
735 CO_2 on phytoplankton during a mesocosm experiment in the southern eutrophicated coastal
736 water of China. Scientific reports, 7(1), 6868. https://doi.org/10.1038/s41598-017-07195-8
737 Mehrbach, C., Cuberson, C.H., Hawley, J.E., Pytkowicz, R.M., 1973. Measurements of the apparent
738 dissociation constants of carbonic acid in seawater at atmospheric pressure. Limnol. Oceanogr.
739 18, 897–907.
740 Myklestad, S.M., 2000. Dissolved organic carbon from phytoplankton. Mar Chem 5:112–144.
741 https://doi.org/10.1016/j. marchem.2009.01.001.
742 Nixon, S.W., 1995. Coastal marine eutrophication: a definition, social causes, and future concerns,
743 Ophelia. v. 41, p. 199–219.

Oliveira, M.L.P., 2013. Análise da hidrodinâmica do sistema lagunar de Saquarema frente às projeções de aumento do nível médio do mar. Programa de Pós-graduação e Pesquisa de Engenharia. Universidade Federal do Rio de Janeiro. Dissertação de mestrado. 102p.

Pereira, E.R.C., 1991. Estudo Experimental da Influência do Sedimento sobre as Atividades Metabólicas na Laguna de Saquarema - RJ. Dissertação de Mestrado. Niterói: Programa de Geoquímica, UFF.

Pierrot, D., Lewis, D.E., Wallace, D.W.R., 2006. MS Excel Program Developed for CO_2 System Calculations. ORNL/CDIAC-105a. Carbon Dioxide Information Analysis Center, Oak Ridge National Laboratory, U.S. Department of Energy, Oak Ridge, Tennessee. Doi: 10.3334/CDIAC/otg.CO2SYS_XLS_CDIAC105a.

Phlips, E.J., Badylak, S., Grosskopf, T., 2002. Factors Affecting the Abundance of Phytoplankton in a Restricted Subtropical Lagoon, the Indian River Lagoon, Florida, USA. Estuarine, Coastal and Shelf Science 55 (3), 385-402 doi:10.1006/ecss.2001.0912.

Pritchard, D.W., 1967. Observation of circulation in coastal plain estuaries. In: Lauff GH, editor. Estuaries, Washington, DC: American Association for the Advancement of Science, pp.3-5.

Rabalais, N. N., Turner, R. E., Díaz, R.J., Justić, D., 2009. Global change and eutrophication of coastal waters. ICES Journal of Marine Science, 66 (7) 1528–1537, https://doi.org/10.1093/icesjms/fsp047.

Raymond, P.A. and Cole, J.J., 2001. Gas Exchange in Rivers and Estuaries: Choosing a Gas Transfer Velocity. Estuaries, v. 24, n. 2, p. 312.

Ribas-Ribas, M., Hernández-Ayón, J.M., Camacho-Ibar, V.F., Cabello-Pasini, A., Mejia-Trejo, A., Durazo, R., Galindo-Bect, S., Souza, A.J., Forja, J.M., Siqueiros-Valencia, A., 2011. Effects of upwelling, tides and biological processes on the inorganic carbon system of a coastal lagoon in Baja California. Estuarine, Coastal and Shelf Sci 95(4): 367–376.

Sabine, C.L., Feely, R.A., Gruber, N., Key, R.M., Lee, K., Bullister, J.L., Wanninkhof, R., Wong, C.S., Wallace, D.W.R., Tilbrook, B., Millero, F.J., Hung Peng, T., Kozyr, A., Ono, T., Rios, A.F., 2004. The Oceanic Sink for Anthropogenic CO_2. Science 305(5682):367–71.

Sathyendranath, S., Stuart, V., Nair, A., Oka, K., Nakane, T., Bouman, H., Forget, M.H., Maass, H., Platt, T., 2009. Carbon to chlorophyll ratio and growth rate of phytoplankton in the sea. Mar Ecol Prog Ser 383:73–84. https://doi.org/10.3354/meps07998.

Strickland, J.D.H. and Parsons, T.R., 1972. A practical handbook of seawater analysis. Fisheries Research Board of Canada Bulletin, 167.

Wanninkhof, R., 1992. Relationship between wind speed and gas exchange. J. Geophys. Res. 97, 7373–7382. https://doi.org/10.1029/92JC00188.

778 Weiss, R.F., 1974. Carbon dioxide in water and seawater: the solubility of a non-ideal gas, Mar.
779 Chem., 2, 203–215.
780 Wollast, R., 1991. The coastal organic carbon cycle: fluxes, sources and sinks. In: Montoura, R.F.C.,
781 Martin, J.M., Wollast, R. (Eds.). Ocean margin processes in global change. [S.l.]: Wiley
782 Intersciences Publishers. p. 365-381.
783
784
785

786 **Table 1**. Mean (± standard deviation), minimum and maximum of the principal physicochemical
787 parameters of the waters of Saquarema Lagoon for the sampling periods.
788

	November 2019		February 2020	
	Spatial sampling	Temporal sampling (12h)	Spatial sampling	Temporal sampling (24h)
Temperature (°C)	24.17 ± 0.77 (22.19 - 25.42)	23.01 ± 0.27 (19.8 - 23.5)	29.56 ± 1.14 (26.26 - 32.3)	20.74 ± 4.62 (16.33 -30.03)
Salinity	25.25 ± 4.64 (16.17 - 31.92)	29.37 ± 0.71 (27.87 - 30.2)	20.43 ± 5.63 (14.32 - 30.85)	32.05 ± 2.32 (28.11 - 34.47)
pCO_2 (ppmv)	177 ± 73 (60 - 301)	253 ± 19 (222 – 280)	126 ± 52 (60 - 249)	357 ± 150 (183 - 529)
SPM (mg L^{-1})	29.9 ±7 .6 (20.5 - 44)	25.5 ± 23.9 (9.5 - 98.7)	43.7 ± 24.7 (14 - 118.5)	20.2 ± 8.3 (8.7 - 42.5)
DOC (mg L^{-1})	9.2 ± 3.3 (4.7 - 14.3)	5.4 ± 0.8 (4.6 - 6.5)	15.6 ± 4.6 (6.3 - 19.8)	5.0 ± 3.8 (1.0 - 10.3)
POC (mg L^{-1})	6.0 ± 2.0 (3.4 - 9.8)	3.5 ± 0.6 (2.5 - 4.4)	8.6 ± 3.3 (3.3 - 12.3)	2.8 ± 2.5 (0.4 - 6.6)
POC (%of SPM)	20.3 ± 4.9 (12.2 - 28.4)	19.8 ± 6.5 (5.71 - 29.6)	22.0 ± 7.3 (8.3 - 31.2)	11.5 ± 8.3 (2.42 - 26.3)
Chl-*a* (µg L^{-1})	22.9 ± 14.9 (7.6 - 77.1)	15.7 ± 3.3 (7.3 - 31.5)	138.1 ± 56.6 (35.8 - 217.1)	16.1 ± 13.8 (2.7 - 36.0)
TA (µmol kg^{-1})	2007 ± 213 (1705 - 2319)	2229 ± 24 (2188 - 2265)	1762 ±246 (1466 - 2229)	2253 ± 105 (2098 - 2376)
DIC (µmol kg^{-1})	1717 ± 255 (1287 - 2071)	1897 ± 14 (1869 - 1920)	1373 ± 248 (1091 - 1816)	1998 ± 203 (1748 - 2211)
Ω Calcite	6.5 ± 1.8 (1.8 – 8.7)	6.0 ± 0.4 (5.5 – 6.6)	6.9 ± 0.8 (5.2 – 8.3)	5.2 ± 1.9 (3.4 – 7.8)
Ω Aragonite	4.1 ± 1.1 (1.1 – 5.3)	3.9 ± 0.3 (3.6 – 4.3)	4.3 ± 0.6 (5.3 – 3.1)	3.4 ± 1.3 (2.2 – 5.1)

789
790
791
792
793

Table 2. Mean values measured in situ of ΔpCO_2 (pCO_{2water} - pCO_{2air}) and wind speed at 10 m height (U10). Calculated mean values for gas exchange coefficient (k_{600}) and CO_2 fluxes at the air-water interface in each sampling campaign. W92 is the data calculated according to k600 of Wanninkhof (1992), RC01 is the data calculated according to k600 of Raymond and Cole (2001), and A09 is data calculated according to k600 of Abril et al. (2009).

		Nov. 2019		Feb. 2020		
		Spatial sampling	Temporal sampling	Spatial sampling	Temporal sampling (ebb tide)	Temporal sampling (flood tide)
ΔpCO_2 (ppmv)		-233±73	-157±19	-283±52	-192±40	94±68
U10 (m s^{-1})		2.03±0.89	2.83±0.64	2.8±1.02	1.46±0.51	1.69±1.02
k_{600} (cm h^{-1})	W92	1.4±0.3	2.5±0.2	2.4±0.5	0.8±0.1	1.1±0.5
	RC01	3.9±2.6	5.1±2.4	5.1±2.7	3.2±2.3	3.4±2.7
	A09	7.0±4.1	9.0±3.4	9.0±4.4	5.5±3.1	6.1±4.4
FCO_2 (mmol C m^{-2} h^{-1})	W92	-0.9±0.9	-1.2±0.1	-2.5±0.5	-0.4±0.2	0.2±0.3
	RC01	-2.5±2.3	-2.6±0.3	-5.2±1.1	-1.5±0.9	0.8±1.0
	A09	-4.5±4.2	-4.5±0.5	-9.2±2.1	-2.7±1.6	1.4±1.8
	Average	-2.6±4.8	-2.7±0.5	-5.6±2.4	-4.6±1.8	0.8±2.1

Table 3. Comparison of the values of DOC, POC, Chl *a* observed during the study with values in the late 80's and 90's.

	Pereira (1991)		**This study**	
	Jardim*	Fora#	Jardim	Fora
DOC	12.6±3.5	8.6±2.6	13.8±5.6	7.5±2.5
POC	7.1±1.4	1.7±0.3	8.7±2.9	4.1±0.9
Chl-a	16.7±10.3	13.3±3.3	116.8±85.2	45.2±23.4

*from Mar. 89 to Jul.89; # from Oct.89 to Jan.90

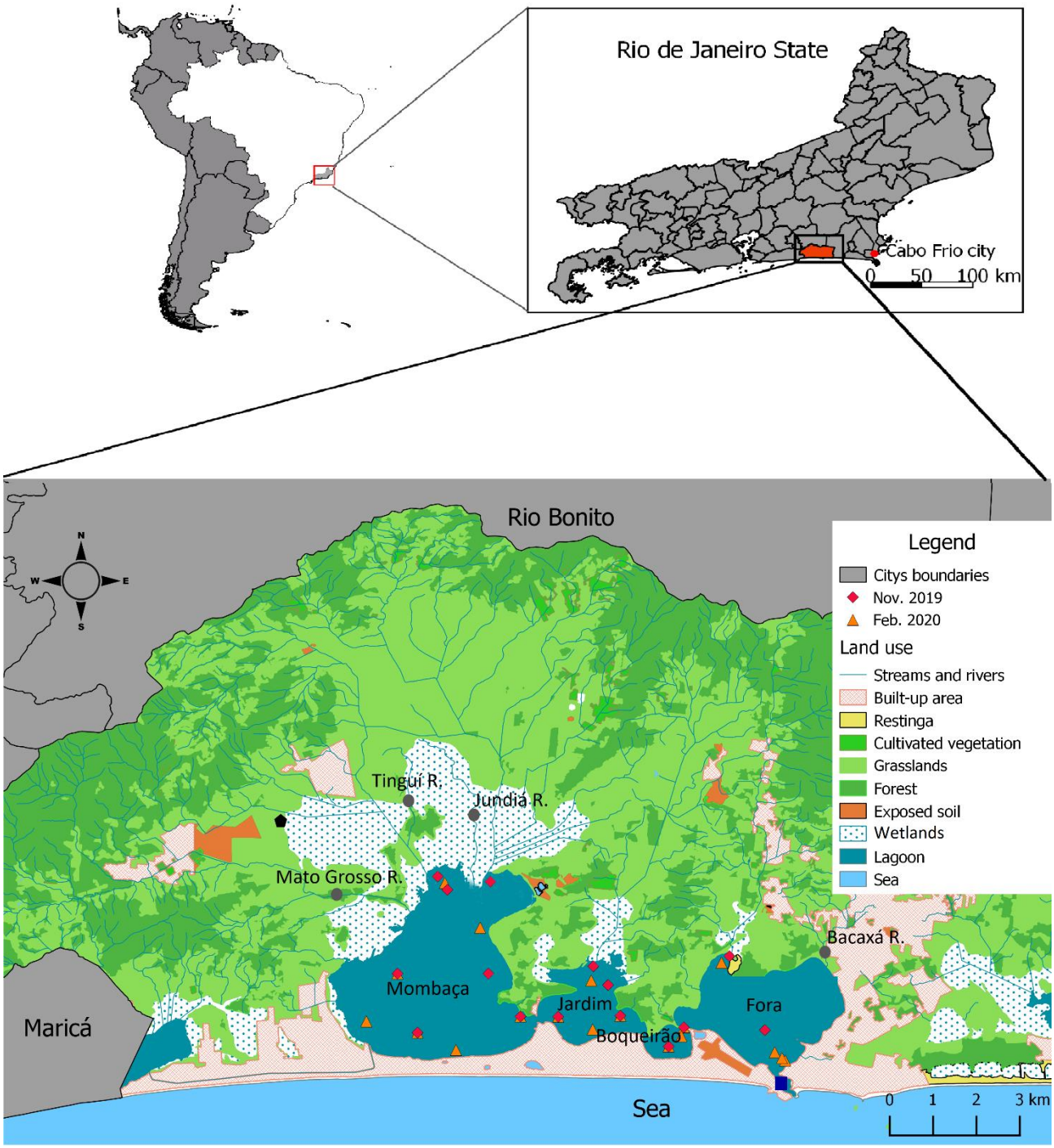

811

812

813 **Figure 1**. Map of land use and occupation of the watershed of the Saquarema Lagoon. The red
814 diamonds represent the sampling stations during the first campaign (Nov 2019), the orange triangles
815 represent the sampling stations during the second campaign (Fev 2020), the blue square represent the
816 temporal monitoring , black point represents the Sampaio Correa meteorological station (22.87° S,
817 42.61°W) where wind speed was measured and the grey points indicate the sampled river stations.

818

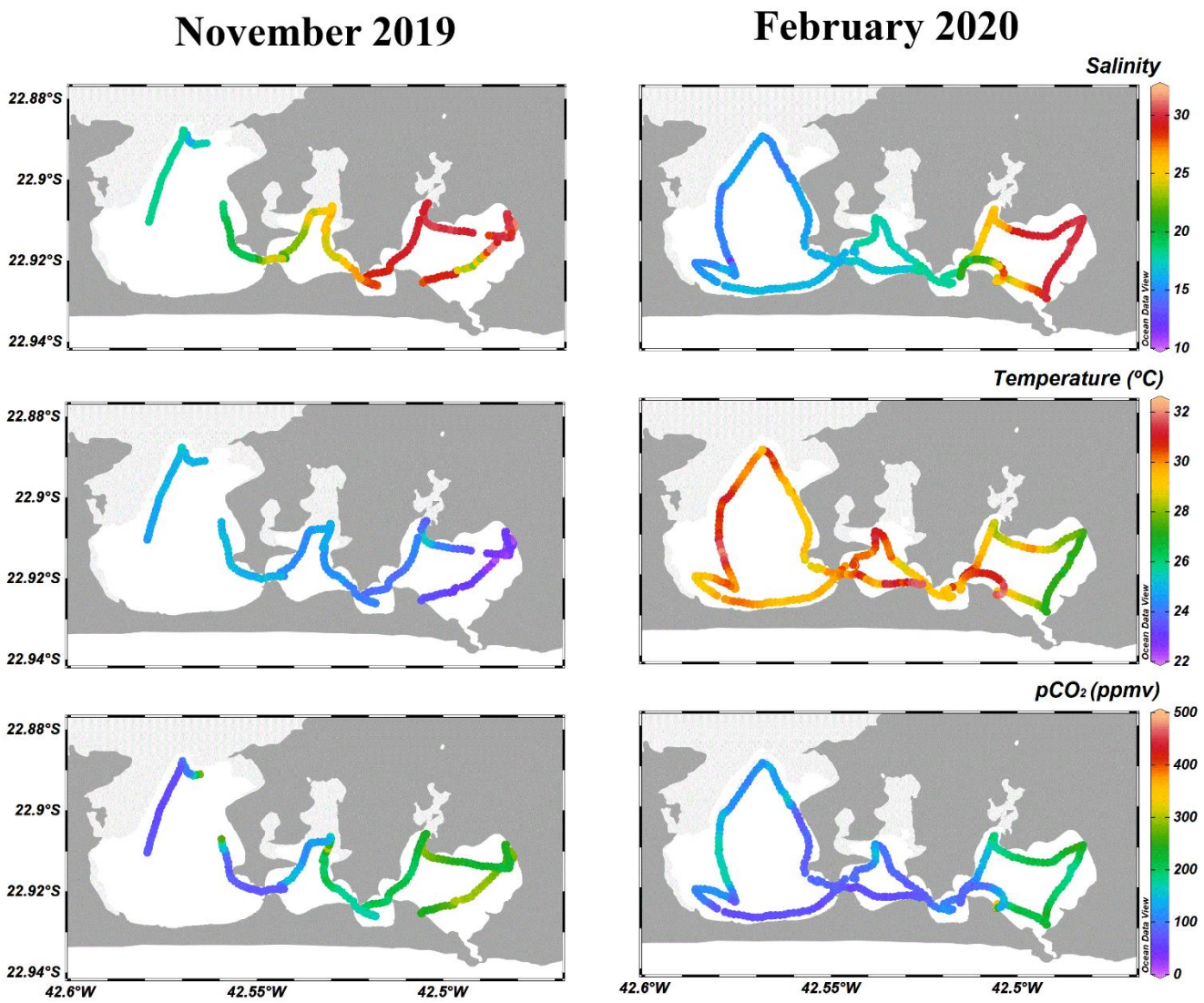

Figure 2. Maps showing the boats tracks and the spatial continuous measurements of salinity, temperature and pCO_2 in surface waters of Saquarema lagoon for both sampling campaigns in Nov 2019 - and Feb 2020.

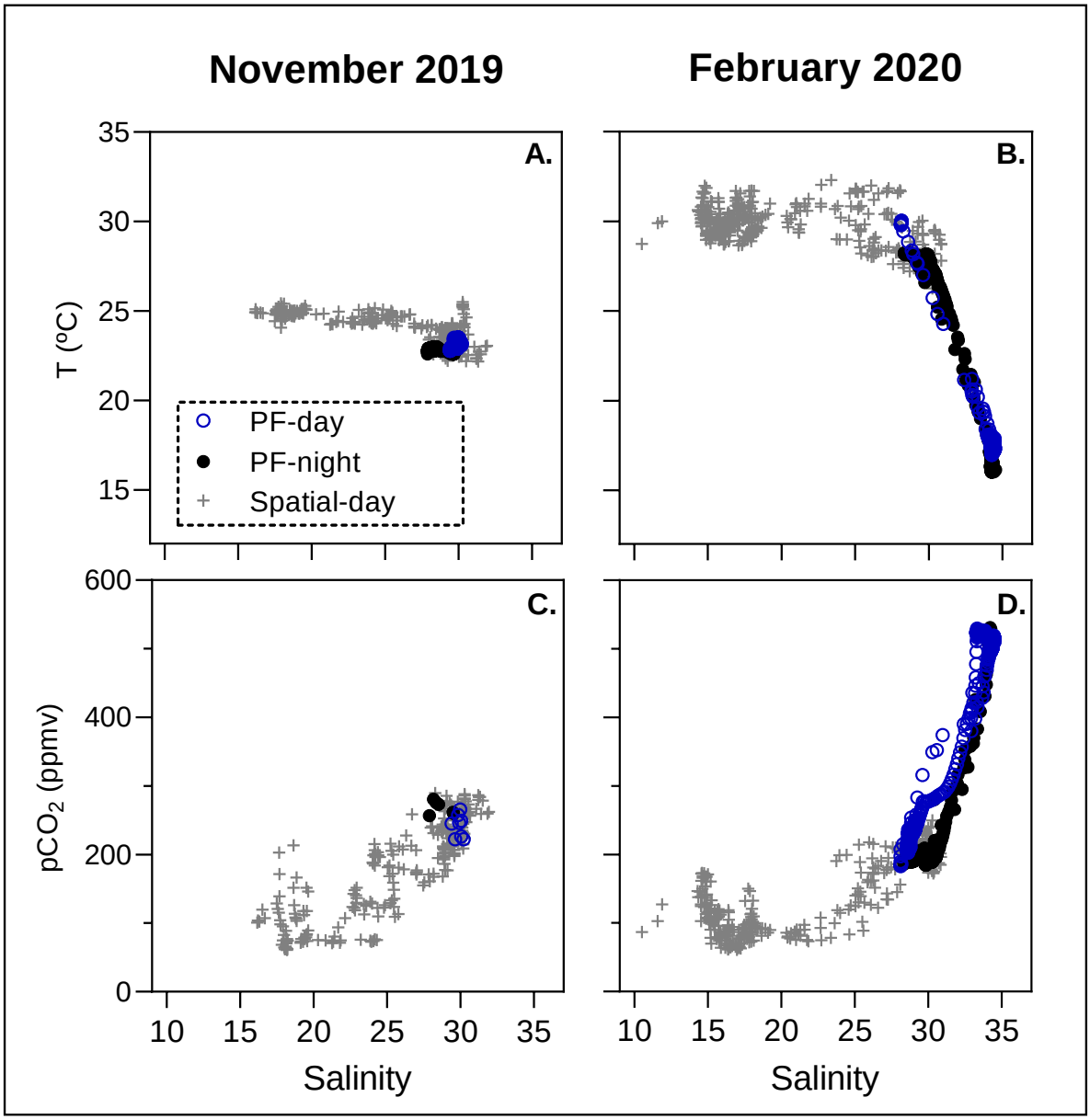

Figure 3: Distribution of pCO_2 and temperature as a function of salinity during the spatial and temporal monitoring for the two campaigns. "FP" refers to fixed point monitoring at the lagoon outlet, "Spatial" to spatial monitoring during the day inside the lagoon.

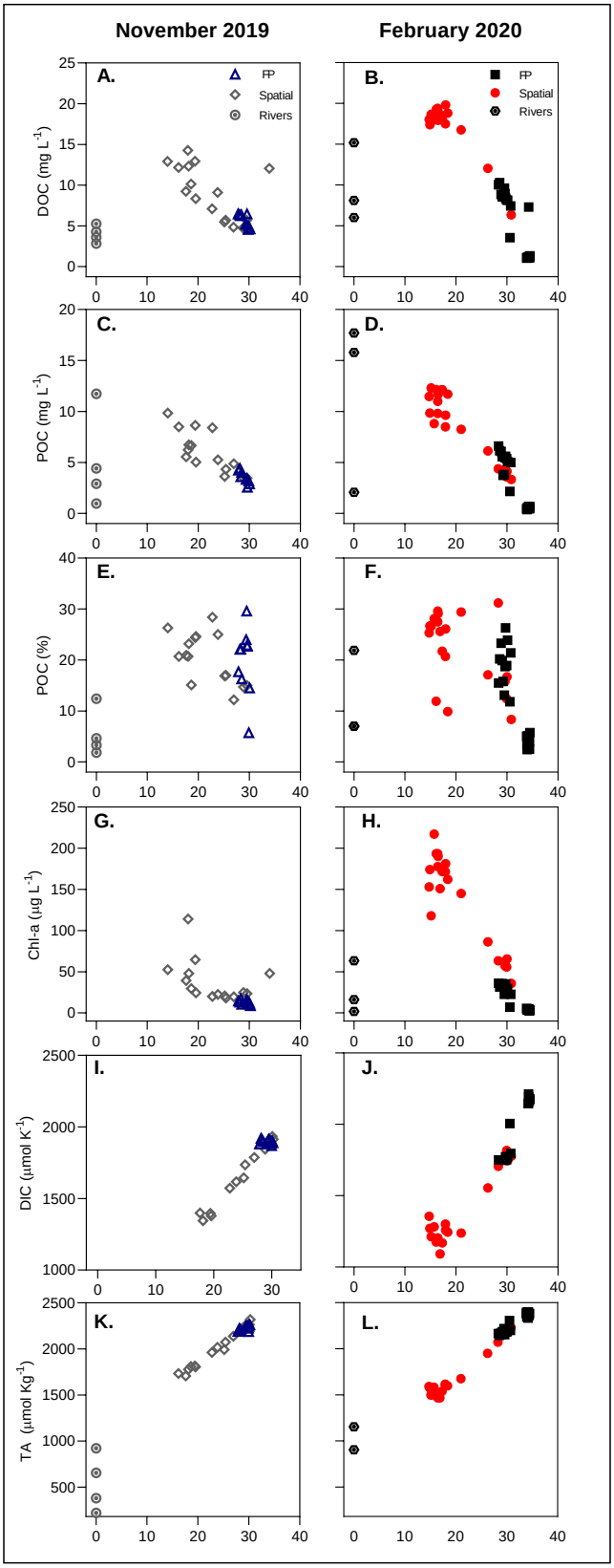

844

845 **Figure 4:** Distributions of DOC, POC, POC %, Chl *a*, DIC, TA as a function of salinity for the two
846 samplings. "FP" refers to fixed point monitoring at the lagoon outlet, "Spatial" to spatial monitoring
847 during the day inside the lagoon.

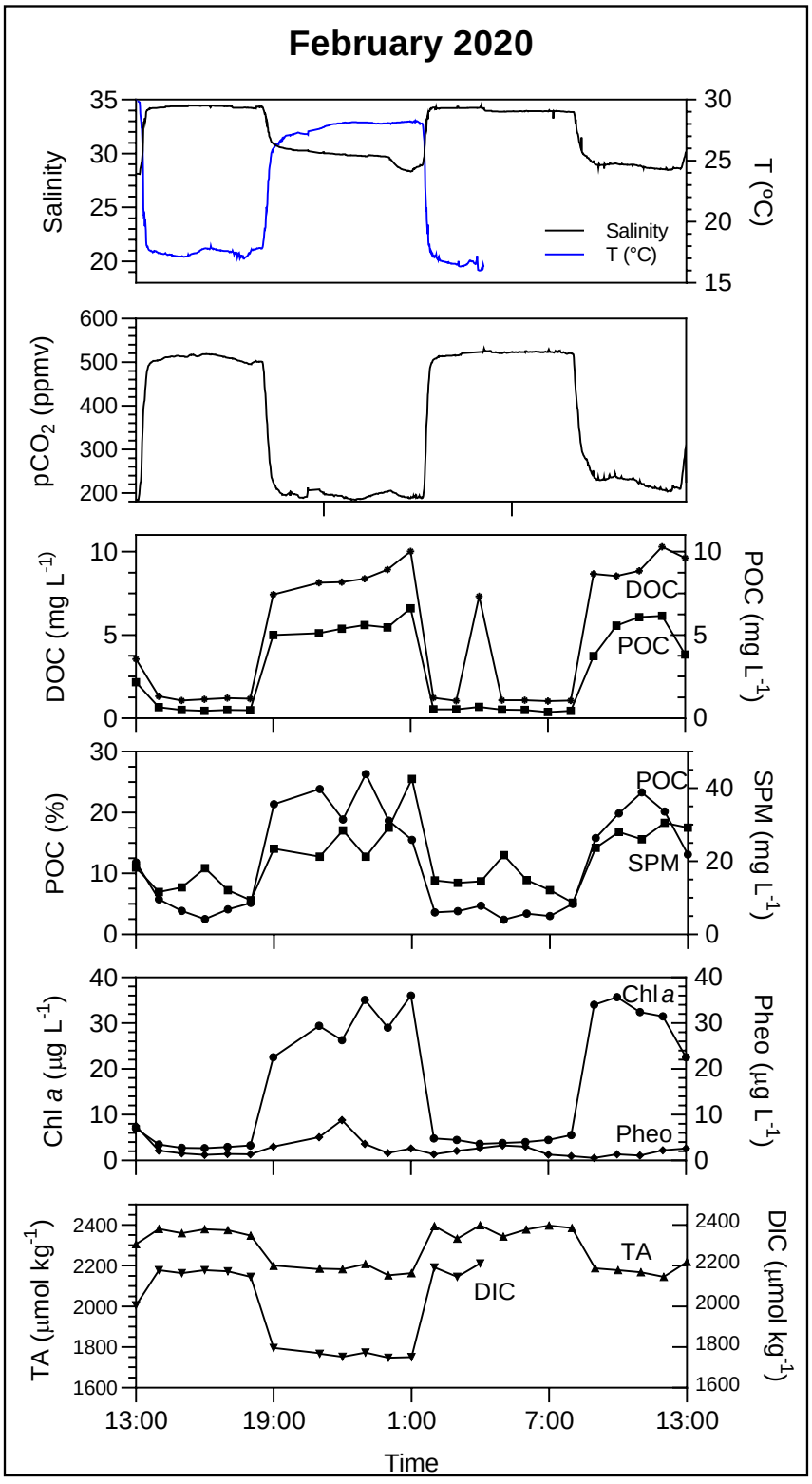

848

849 **Figure 5:** Diurnal variation of the concentrations of the main water parameters at the mouth of the
850 lagoon during Feb. 2020. Note that a temporal monitoring of 12h was also performed in Nov. 2019,
851 but the parameters were relatively constant, and the average values are reported in Table 1.

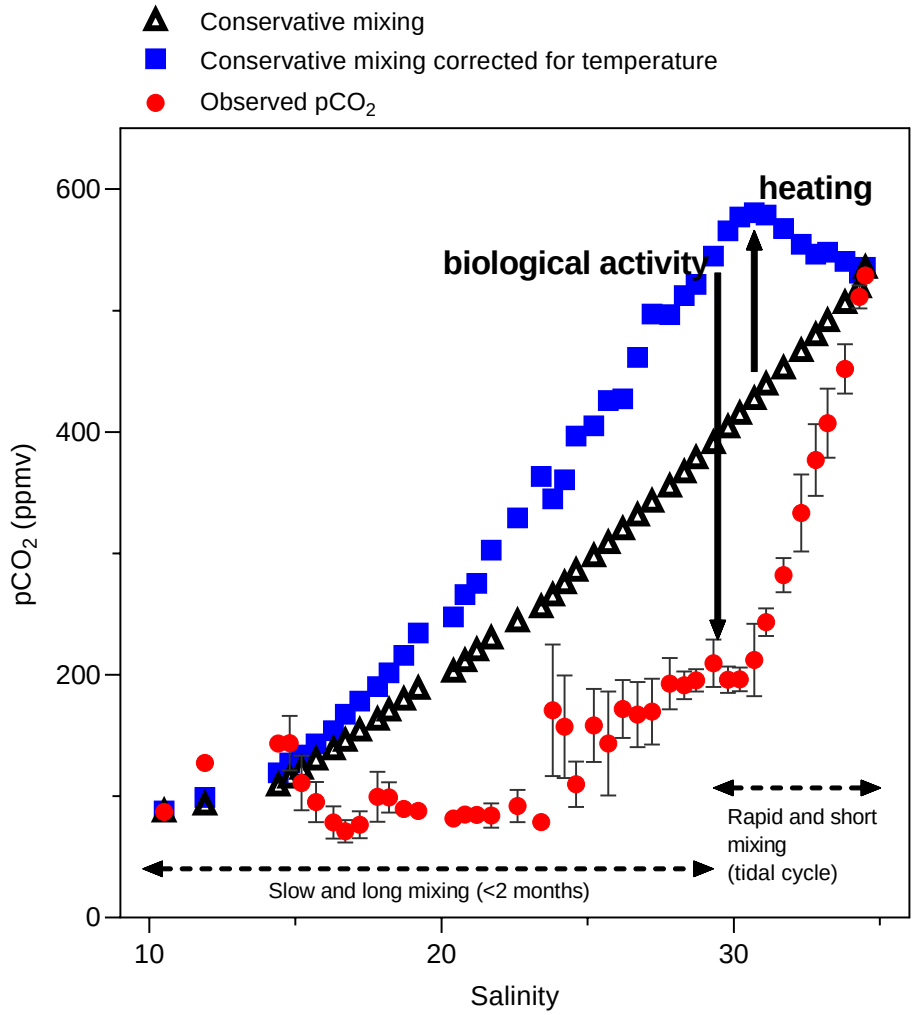

Figure 6: Comparison of observed water pCO_2 (red) with the results of the mixing model of South Atlantic Central Water (Salinity 34.6) with lagoon waters (Salinity 10). The "conservative mixing" curve (black) is calculated by considering TA, DIC and temperature conservativity between the two end-members; The "conservative mixing corrected for temperature" curve (blue) is calculated by considering TA, DIC conservativity between the two end-members and the observed temperature along the salinity gradient.

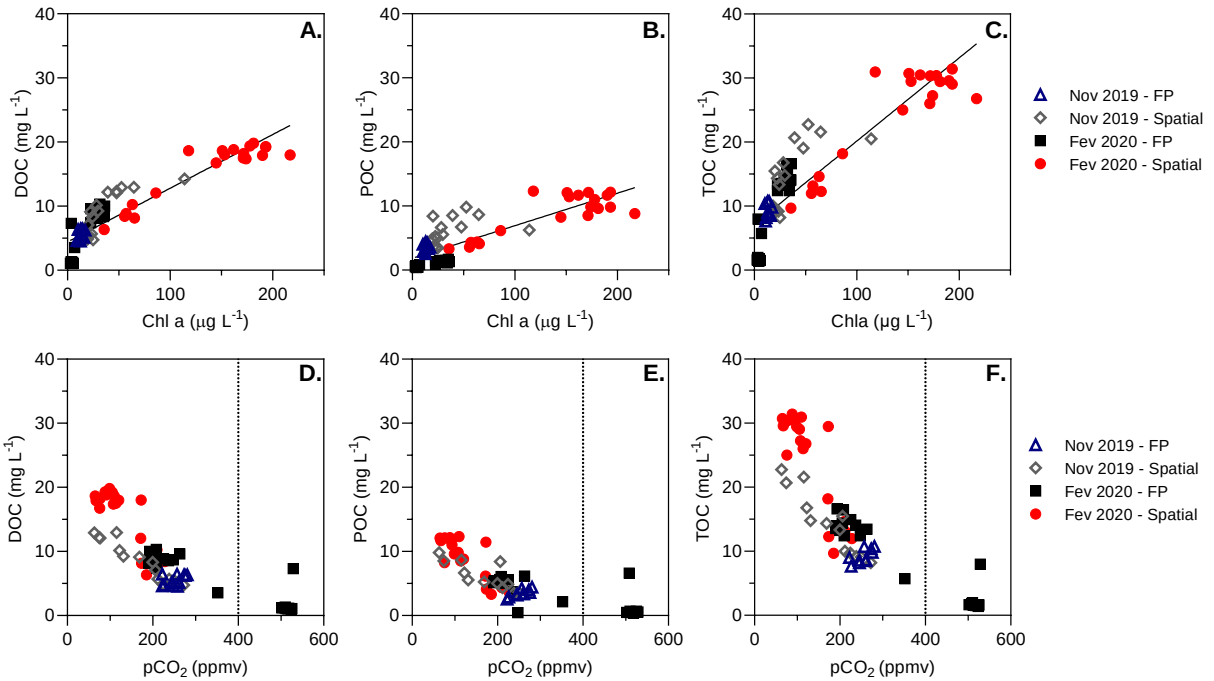

Figure 7: Relationships between: (A) DOC versus Chl *a*; (B) POC versus Chl *a*; (C) TOC versus Chl *a*; (D) DOC and pCO_2; (E) POC and pCO_2; (F) TOC and pCO_2. The dashed lines at 400 ppmv represent the global average atmospheric CO_2 concentration. "FP" refers to fixed point monitoring at the lagoon outlet, "Spatial" to spatial monitoring during the day inside the lagoon.

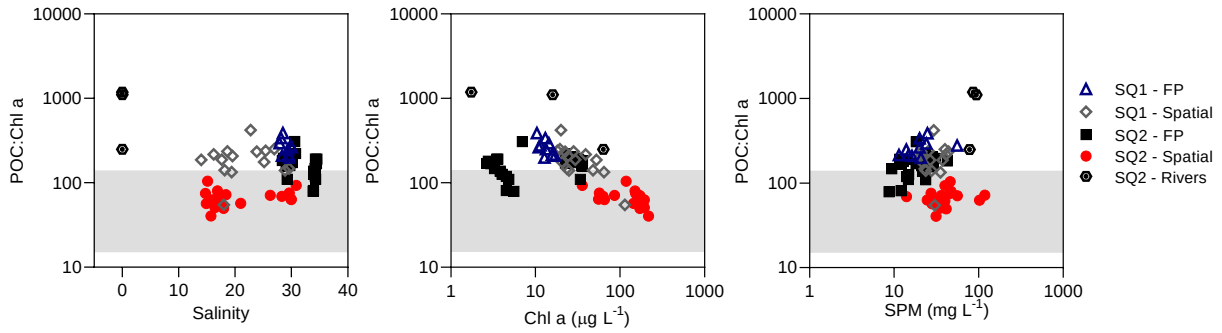

Figure 8: plots of (A) POC% (percent of SPM) versus SPM; (B) POC:Chl *a* vs Chl *a*, of the two samples campaigns for the spring and summer. The shaded area represents POC:Chl *a* range for living phytoplankton. “FP” refers to the monitoring at fixed point at the lagoon outlet, “Spatial” to spatial monitoring during the day inside the lagoon.

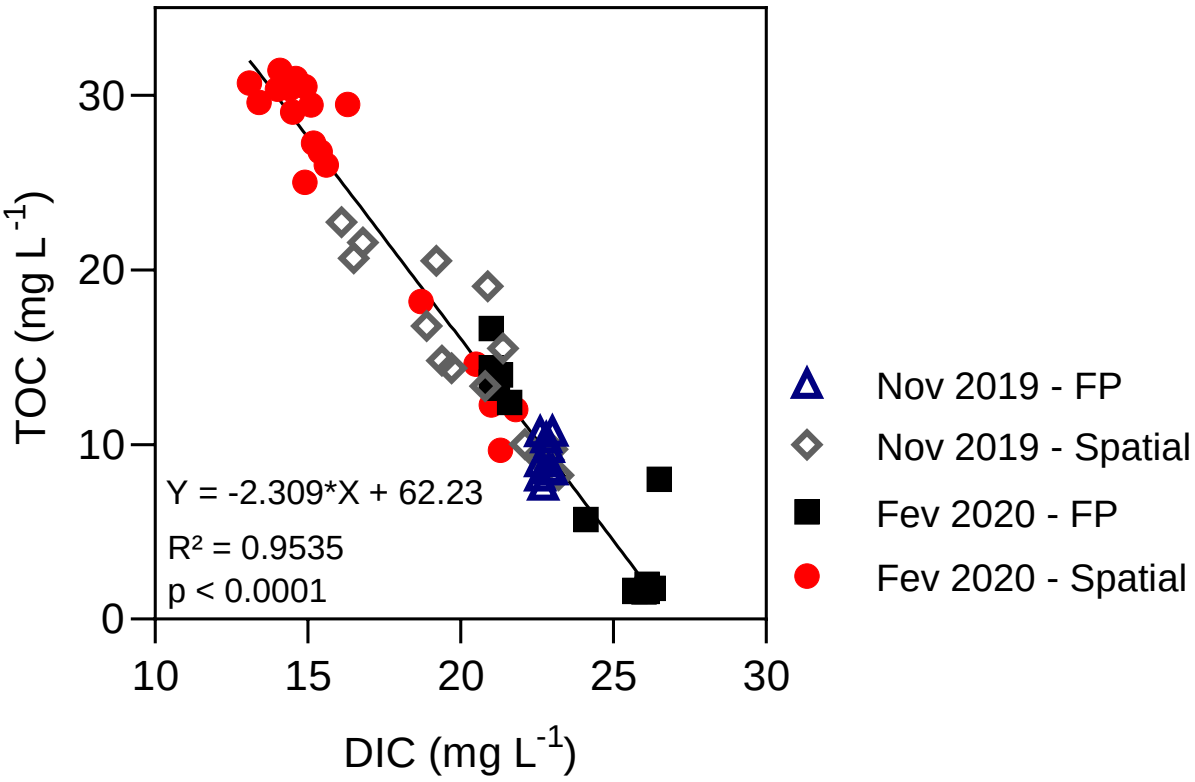

897

898

899 **Figure 9**: Linear Regression between DIC and TOC for the two sampling campaigns.

900

Table S1: Statistical analysis comparing the spatial variation of parameters measured between different lagoon's compartments.

		Mombaça	Fora	Jardim		Mombaça	Fora	Jardim
ANOVA	**Salinity**				**TA**			
	Mombaça	-			Mombaça	-		
	Fora	**< 0.001**	-		Fora	**< 0.001**	-	
	Jardim	**< 0.001**	**< 0.001**	-	Jardim	**< 0.01**	**< 0.001**	-
	SPM							
	Mombaça	-						
	Fora	> 0.05	-					
	Jardim	> 0.05	> 0.05	-				
kruskall-Wallis	**Temperature**				**DOC**			
	Mombaça	-			Mombaça	-		
	Fora	> 0.05	-		Fora	**< 0.001**	-	
	Jardim	> 0.05	> 0.05	-	Jardim	> 0.05	**< 0.01**	-
	Chla				**DIC**			
	Mombaça	-			Mombaça	-		
	Fora	> 0.05	-		Fora	**< 0.001**	-	
	Jardim	> 0.05	> 0.05	-	Jardim	> 0.05	**< 0.01**	-
	POC				**pCO_2**			
	Mombaça	-			Mombaça	-		
	Fora	**< 0.001**	-		Fora	**< 0.01**	-	
	Jardim	> 0.05	**< 0.001**	-	Jardim	> 0.05	**< 0.001**	-

Table S2: Statistical analysis comparing the two sampling periods, November 2019 and February 2020.

	Mann-Whitney	ANOVA
Temperature (°C)	>0.05	
Salinity		< 0.001
pCO_2 (ppmv)	<0.001	
SPM (mg L^{-1})		>0.05
DOC (mg L^{-1})	<0.0001	
POC (mg L^{-1})	<0.0001	
Chl-*a* (µg L^{-1})	<0.001	
TA(µmol kg^{-1})		< 0.001
DIC (µmol kg^{-1})	<0.0001	